J. Cent. South Univ. (2022) 29: 2502−2512
DOI: https://doi.org/10.1007/s11771-022-5092-8

Springer

Cyclic test and numerical study of seismic performance of precast segmental concrete double-columns

ZOU Shuang(邹爽)[1, 2], WENLIUHAN Hei-sha(温留汉 黑沙)[1, 2]*, MAO Yong-ping(毛永平)[3], YU Bi-peng(于碧澎)[3], ZHANG Chong-bin(张崇斌)[4]

1. Earthquake Engineering Research & Test Center, Guangzhou University, Guangzhou 510405, China;
2. Key Laboratory of Earthquake Engineering and Applied Technology in Guangdong Province, Guangzhou 510405, China;
3. Jianhua Building Materials (Guangdong) Sales Co., Ltd., Guangzhou 510403, China;
4. China Railway Engineering Design and Consulting Group Co., Ltd., Beijing 100055, China

Abstract: The comparative research on the seismic performance of grouted sleeve connected pier (GS) and prestressed precast segmental concrete pier (PC) is mostly carried out by numerical simulation. In this study, the GS pier and the PC pier of the new railway project from Hetian to Ruoqiang are taken into consideration. Two kinds of 1/5-scale assembled double-column specimens are made, and the quasi-static tests are carried out. The overall seismic performance of the two spliced piers is studied, and compared in terms of failure mechanism, bearing capacity, ductility, stiffness and energy dissipation capacity. The results show that the failure modes of both GS pier and PC pier are characterized by bending. However, the specific failure location and form are different. The GS pier presents a complete hysteretic curve, large equivalent stiffness and strong energy dissipation capacity. The hysteretic area of the PC pier is small. However, it has good self-reset ability and quasi-static residual displacement. Finite element models are set up using DispBeamColumn fiber elements and ZeroLength elements. The models that are calibrated with the test data can effectively simulate the damage development under monotonic loading. The load−displacement curves are in good agreement with the backbone curves of the test results.

Key words: pseudo static test; seismic performance; prestressed precast segmental concrete; double-column piers; steel sleeve connection; precast concrete prestressed steel

Cite this article as: ZOU Shuang, WENLIUHAN Hei-sha, MAO Yong-ping, YU Bi-peng, ZHANG Chong-bin. Cyclic test and numerical study of seismic performance of precast segmental concrete double-columns [J]. Journal of Central South University, 2022, 29(8): 2502−2512. DOI: https://doi.org/10.1007/s11771-022-5092-8.

1 Introduction

There are many connection types available for the precast assembly pier system, and the precast assembly pier system formed by different connection modes has different characteristics in seismic performance [1−8]. The seismic performance of a segmental pier depends on the connection type [9−12]. According to the required seismic performance, the precast assembly pier system can be basically divided into two types: the "equivalent conventional monolithic bridge columns" (ECMB) and the "non-equivalent

Foundation item: Project(N2018G034) supported by China Railway Corporation
Received date: 2021-06-15; **Accepted date:** 2021-09-09
Corresponding author: WENLIUHAN Hei-sha, PhD, Professor; E-mail: wen.liuhan@a-sys.co.jp; ORCID: https://orcid.org/0000-0001-6251-2237

conventional monolithic bridge columns" (NECMB) [13−14]. ECMB refers to the precast pier formed on site with a connection type that can ensure the same or similar seismic performance with the one of the traditional cast-in-place pier, including horizontal bearing capacity, deformation capacity, stiffness and energy dissipation capacity [15−16]. Among them, the grouting sleeve connection has the advantages of clear force transmission mechanism, less on-site pouring work and faster construction. In order to study the seismic performance of the grouting sleeve connection, a series of quasi-static tests was carried out by LI et al [8], HABER et al [17] and AMELI et al [18]. The main conclusions include that the deformation capacity of the precast pier with sleeve grouting is slightly smaller than that of the cast-in-place pier with the same parameter [19 − 21]. QU et al [22] conducted quasi-static tests on double columns with sleeve grouting connection, which proved that sleeve grouting is also a feasible connection method for pier cap beam connection.

The NECMB mainly connects the pier segments as a whole by prestressed tendons. The pier components remain elastic in the earthquake, and the prestressed tendons provide self-reset ability. This kind of pier has significant advantages of rapid construction, and has been widely used in bridges in non-seismic areas [23−24]. For NECMB, HEWES et al [25], GE et al [26] and JIA et al [27] carried out low-cycle reciprocating tests and found that the NECMB without special energy dissipation measures has nonlinear elastic hysteretic behavior and small residual deformation after loading, but poor energy dissipation capacity.

Considering that both ECMB and NECMB are widely used in engineering projects, it is necessary to carry out comparative study on their seismic performance. In this paper, taking the actual railway pier as the research object, two models are designed, assuming a scale of 1: 5, for the two connection forms of grouting sleeve and prestressed tendons. The displacement hysteretic curves, residual displacement and other indicators are obtained through quasi-static test energy consumption.

2 Pier prototypes

This paper studies the seismic performance of a double-column segmental railway pier which was designed for the new railway project from Hetian to Ruoqiang in the southern part of the Taklimakan Desert in Hetan City, Xinjiang, China. The 8 m grouting sleeve connection pier and 15 m prestressed connection pier in Hetian-Ruoqiang railway line are taken as the research objects. The seismic performance of GS pier and PC pier is compared and analyzed through the scale quasi-static test under the condition of the same axial compression ratio [28].

2.1 GS pier

Figure 1 shows the prototype GS pier considered in this study. The cap beam has a rectangular cross section of 2.4 m×1.3 m with length of 5.6 m. The whole pier body of the GS pier is prefabricated as one segment. The cap beam, pier body segment and bearing platform are prefabricated separately and steel sleeves are embedded at the top and bottom of columns. Grouted sleeves are used for the connection of the segments. During the assembling procedure, the steel sleeves work as reserved reinforcements embedded in the columns, the cap beam and the bearing platform one by one as shown in Figure 2. After the pier body is positioned, grouting is applied at the sleeves through the embedded grouting holes.

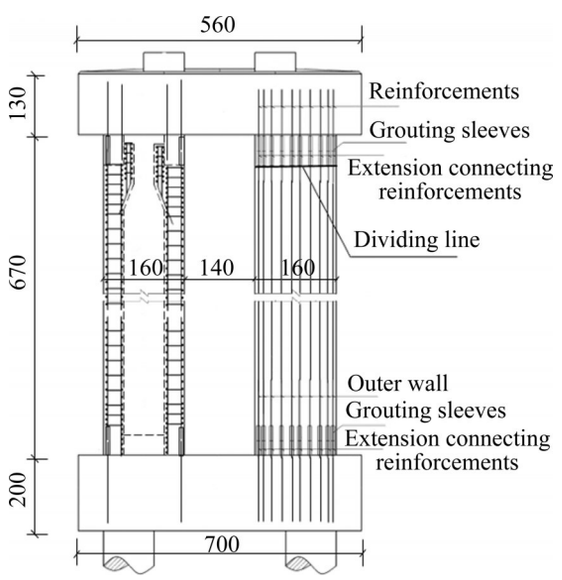

Figure 1 Prototype of the GS pier (unit: cm)

2.2 PC pier

The PC pier is shown in Figure 3. The pier body is prefabricated in two segments. Cap beam

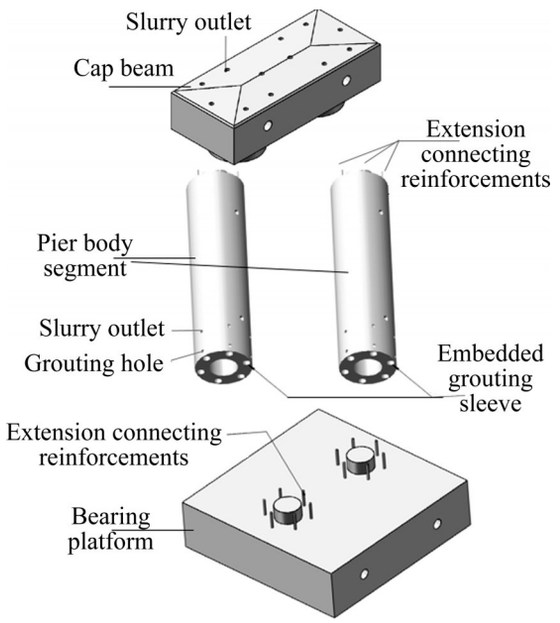

Figure 2 Construction procedure of GS pier

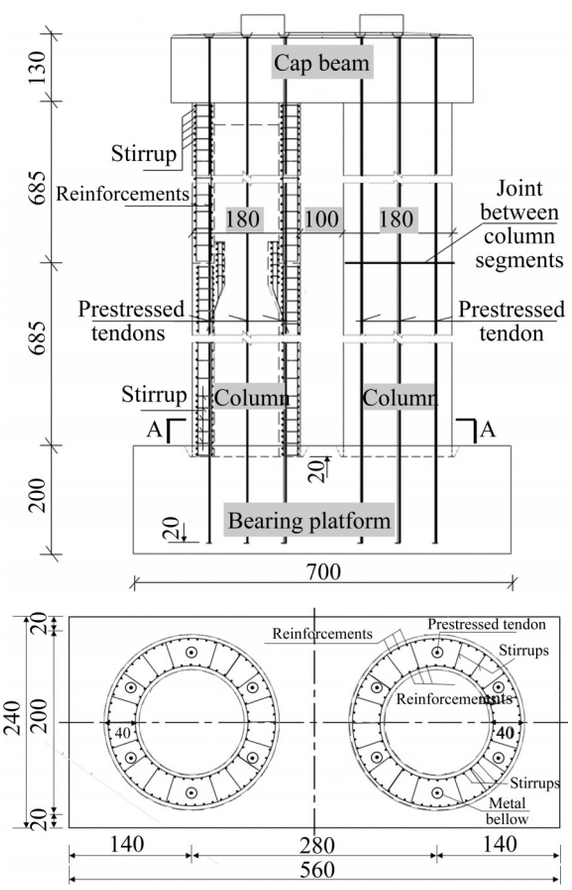

Figure 3 Prototype of the PC pier (unit: cm)

and bearing platform are also prefabricated, separately. The longitudinal reinforcement does not run through the whole pier and the prestressed tendons are used to connect the segments. 12 steel strands with diameter of 15.2 mm are used to form the self-anchored prestressed system. The tensile stress of each steel strand is 1209 MPa. The construction details of the PC pier are shown in Figure 4.

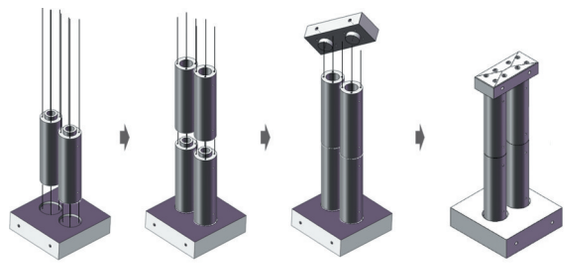

Figure 4 Construction procedure of PC pier: (a) Positioning of lower segment; (b) Positioning of upper segment; (c) Positioning of cap beam; (d) Pretension application

The metal bellows are embedded in the bearing platform, pier body segments and cap beam to form the duct during the prefabricating process.

The prestressed tendons pass through the ducts of the bearing platform; their lower ends are anchored 20 cm above the bottom fiber of the bearing platform.

After the positioning of the two pier body segments in turn, the tendons are threaded along the reserved ducts inside the pier body from bottom to top (Figures 4(a) and (b)).

After the cap beam is in place, the tendons are threaded along the ducts inside the cap beam from bottom to top (Figure 4(c)). Pretension is applied at the top of the cap beam and grouting seals the anchorage from the bottom (Figure 4(d)).

Cement mortar is poured at the upper surface of bearing platform.

2.3 Material properties

The mechanical properties of materials used in the precast segmental pier specimens are shown in Table 1.

3 Cyclic test

3.1 Similarity coefficients

The similarity ratio is set at 1∶5. According to the uniform similarity law [29], the GS and PC pier scale specimens are designed to ensure similar seismic performance between specimens and

Table 1 Properties of the pier specimens

Type	Parameter	Material and layout
GS pier	Longitudinal reinforcement bar	60D25 mm; Yielding stress is 410 MPa
	Strength of concrete	50 MPa
	Grouting material	50 MPa
	Transverse reinforcement bar	D12@100 (Within 1 m of pier bottom); and D12@230 mm; Yielding stress is 410 MPa
PC pier	Prestressed tendon	12D15.2 mm; Yielding stress is 1890 MPa; Initial stress is 1209 MPa
	Longitudinal reinforcement bar	90D12 mm; Yielding stress is 410 MPa
	Transverse reinforcement bar	D12@100 (Within 1 m of pier bottom) and D12@150 mm; Yielding stress is 410 MPa
	Metal bellow	12D85 mm
	Strength of concrete	50 MPa

prototype. The mechanical properties of the materials used for the speicimens are the same as the prototype piers.

3.2 Loading device and loading system

The test setup is shown in Figure 5. The initial axial stress is applied by prestressed tendons to simulate the mass of superstructure. The lower end of the prestressed tendons is anchored at the bearing platform and the upper one passes through the center of the cap beam and is anchored at its top. The vertical load is provided by prestressed tendons, and keep it constant during the whole test process. The axial prestress applied to the top of grouting sleeve test pier is 60 kN, and the axial prestress applied to the top of prestressed test pier is 80 kN. The axial compression ratio of both test piers is the same, equal to 0.2%.

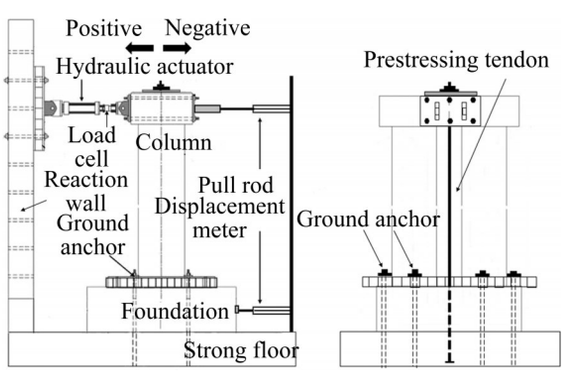

Figure 5 Test setup of pseudo static test of test specimens

The displacement-time history adopts a sine wave mode with increasing amplitude. The amplitude increment is 5 mm. The number of loading steps depends on the damage of each pier itself.

4 Discussion of experimental results

4.1 Failure pattern

The failure modes of both GS and PC specimens show bending characteristics. However, the specific failure parts and forms are different. The failure of the GS specimen can be divided in four stages:

(a) The tensile stress of the concrete at the joint between the pier bottom and the bearing platform leads to the opening of cracks, which close when the columns come back to the equilibrium position (Figure 6(a)).

(b) The cracks expand and widen; then they start to interconnect with each other across the column surface near the bottom joint (Figure 6(b)).

(c) Concrete spalling begins within an area of 100 mm from the column bottom. Crack width reaches up to 4 mm (Figure 6(c)).

(d) The spalling depth increases and the sleeves are exposed. Corner concrete begins to crush. The strength of the specimen begins to degrade up to 85% of the initial ultimate strength (Figure 6(d)). The GS specimen loses its bearing capacity and the test ends.

The joints between the pier body and the bearing platform are subjected to a large force and are damaged and deteriorated under the combination of bending moment and axial force. When the tendons cannot undertake the bending moment, debonding from their anchorage occurs. Further

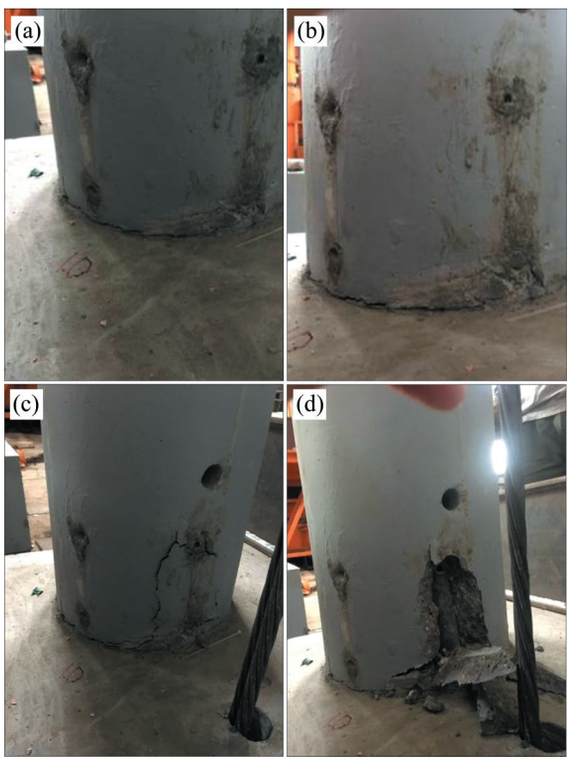

Figure 6 Damage of the GS specimen: (a) Concrete cracking at the joint of pier bottom and bearing platform; (b) Widening of concrete cracking at the joint of pier bottom and bearing platform; (c) The concrete of the outer protective layer at the position of the grouting sleeve is cracked; (d) The concrete of the outer protective layer at the position of the grouting sleeve is peeled off

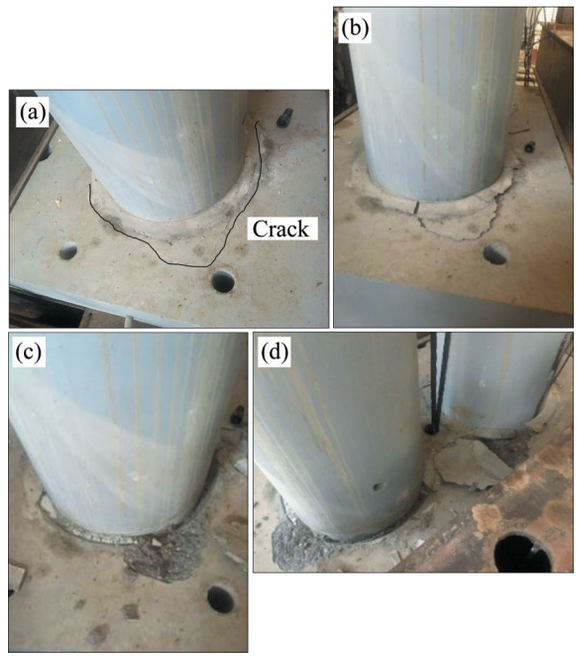

Figure 7 Damage of PC specimens: (a) Cracking of post pouring concrete at the joint of bearing platform and pier column; (b) The crack of post pouring concrete at the joint between bearing platform and pier column is lengthened and widened; (c) The post pouring concrete at the joint between bearing platform and pier column is peeled off; (d) The spalling area of post pouring concrete at the joint of bearing platform and pier column is increased

imposed displacement causes the opening of cracks. The main damage of the GS specimen is that the cracks are irrecoverable and the sleeve is exposed. Slippage or buckling of longitudinal reinforcement bars occurs at the joints, leading to the failure of the specimen.

The failure of the PC specimen is embodied in four stages:

(a) The contact interface between the poured concrete and the bearing platform will crack first. However, these cracks close again when the columns are re-centered (Figure 7(a)).

(b) The cracks expand, widen, and then start to interconnect with each other on the contact surface, forming a complete ring (Figure 7(b)).

(c) Spalling of the poured concrete begins at the bottom of the pier. Gradually, a rocking column mechanism is formed. The pier can be restored at the equilibrium position (Figure 7(c)).

(d) With the increase of horizontal load, the concrete at the bottom of pier column spalls seriously (Figure 7(d)). The prestressed tendons reach the yield stress. The bearing capacity of the specimen suddenly decreases to less than 85% of the maximum value.

As the joint bears a large force, it is the first to be damaged and deteriorated. When the horizontal load is small, the resistance of the pier's base is mainly provided by the cohesive force between the filling concrete and the bearing platform. However, as the horizontal load increases, the joint at the base of the pier opens and cracks appear. The filling concrete gradually loses its cohesive resistance and is peeled off. A rocking column mechanism evolves. The main failure of PC specimen is cracking and spalling at the joint surface of filling concrete and bearing platform.

4.2 Evaluation of experimental results

4.2.1 Hysteretic behaviors

The hysteretic behaviors of the GS and PC

specimens are given in Figure 8. Within the range of 0.02 rad rotation angle of pier top, their hysteresis loops are similar in terms of loading and unloading stiffness, ultimate strength and total area of the curves for both types of piers. Beyond 0.02 rad rotation angle level, the bearing capacity of the GS specimen decreases to 85% of the ultimate load and the experiment ends. The stress of prestressed tendons exceeds the ultimate stress, leading to their fracture. The bearing capacity suddenly drops to 85% from 93% of the previous cycle. After that, the PC specimen still has a certain bearing capacity. The second and third prestressed tendons reach the ultimate stress when the top rotation angle becomes 0.023 rad and 0.029 rad, respectively, leading to a sudden decline of the overall bearing capacity of the PC specimen.

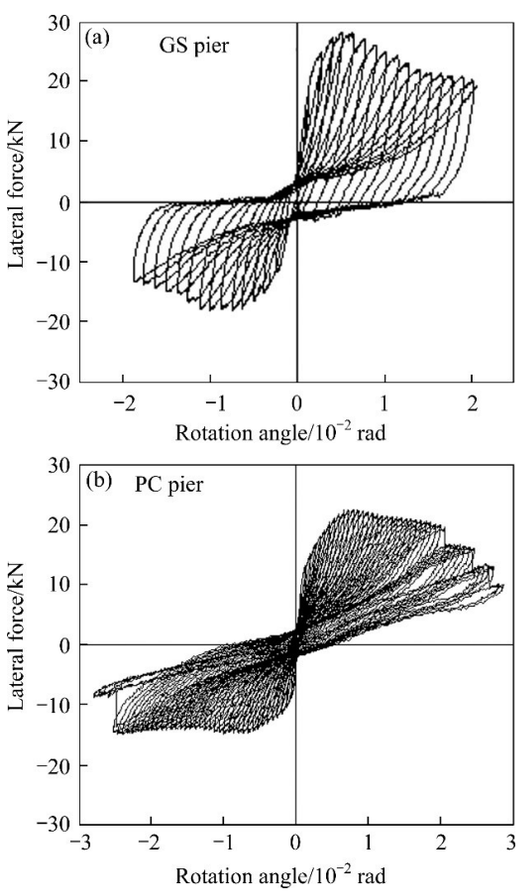

Figure 8 Hysteretic curves of bridge pier specimens

Compared with the prototype pier, the size and stiffness of the bridge pier made after scale reduction are smaller. In the positive loading process, the stiffness in negative direction is affected and weakened. Hence, the area of hysteresis curve in imposed positive displacement is larger than that in negative one for both GS and PC specimens.

4.2.2 Displacement ductility

Displacement ductility is defined as the ratio of the ultimate displacement (δ_u) to the effective yield displacement (δ_y). δ_u is the displacement when the strength decreases to 85% of the ultimate value and δ_y is determined by an equivalent bilinear curve idealized from the force−displacement relationship. The mechanical property parameters and the displacement ductility value (μ) are determined when the ultimate displacement is reached, as shown in Table 2. δ_y is calculated by the general yield moment method [30]. It is noted that the equivalent elastic stiffness K_{eff} values of the two test specimens are basically the same. In this case, the δ_y, yield load F_y and ultimate load F_m of GS specimen are larger than those of PC specimen, but the δ_m is smaller than that of PC specimen, which makes the overall ductility of the PC specimen better than that of GS specimen. This is mainly because the bearing capacity of GS specimen decreases rapidly after reaching the ultimate load, while PC specimen always provides a certain restoring force due to the existence of the tendons until the prestressed tendons are damaged.

Table 2 Critical backbone curve values under the pseudo static test

Specimen	F_y/kN	δ_y/rad	F_m/kN	δ_m/rad	K_{eff}/(kN·rad^{-1})	μ
GS	24	0.003	22	0.011	8193	3.7
PC	16	0.002	19	0.020	8200	10.0

4.2.3 Stiffness degradation

The stiffness ratio parameter λ_i is introduced, as $\lambda_i = \frac{K_i}{K_{eff}}$, where $K_i = (K_i^+ + K_i^-)/2$ $\left(K_i^+ = \frac{F^+_{max}}{\delta^+_{max}},\ K_i^- = \frac{F^-_{max}}{\delta^-_{max}} \right)$. K_i is the average secant stiffness of the specimen under the ith loading cycle; δ^+_{max} and δ^-_{max} are the positive and negative peak displacement respectively; F^+_{max} and F^-_{max} are positive and negative imposed force corresponding to the positive and negative peak displacements, respectively; and K_{eff} is the elastic stiffness of the specimen.

The relationship between the variation λ_i and the rotation angle of the pier bottom is given in

Figure 9. It can be seen that parameter λ_i decreases rapidly with the increase of the rotation angle, for both GS and PC specimens. The PC specimen enters the yield state earlier than the GS specimen. Moreover, after entering the yield state, this parameter λ_i for the GS specimen is always larger than the one for the PC specimen for the same rotation angle. This occurs because the longitudinal reinforcement runs through the whole pier and the joint area of pier body and bearing platform of GS specimen is large. When cracks open and the concrete at the joint reaches yield, the longitudinal reinforcement still contributes to the strength of the cross section, and the pier stiffness decreases slowly. However, only prestressed tendons run through the whole pier of PC specimen, and thus the joint of pier body and bearing platform is weak. Under the application of the horizontal displacement, the concrete at the joint quickly yields, the stiffness decreases rapidly and loses strength. PC specimen reaches the limit state later than GS specimen.

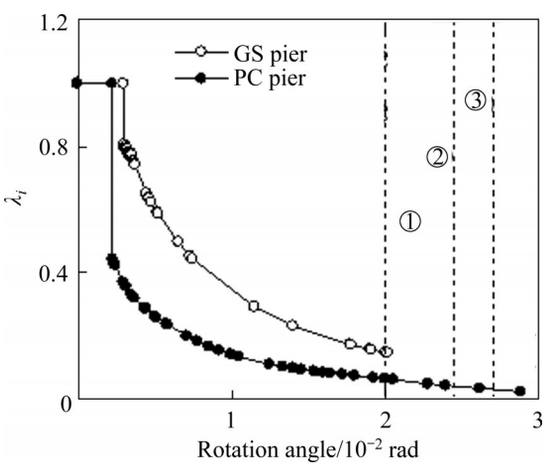

Figure 9 Stiffness degradation (①, ②, ③ represent the first, second and third prestressed tendons reaching the ultimate stress and breaking respectively)

4.2.4 Energy dissipation capacity

The accumulated energy dissipation is calculated based on the area of hysteresis loop at each displacement level. The energy ratio ψ_i is defined as $\psi_i = \dfrac{E_i}{E_{\text{ideal}}}$, where E_i is the hysteretic energy dissipation of one cycle; i is the number of the loading cycle; and E_{ideal} is the hysteretic energy dissipation of an ideal elastoplastic system with the same elastic stiffness as the specimen, $E_{\text{ideal}}=E_i+E_1$.

The relationship of ψ_i with rotation angle is shown in Figure 10. The ψ_i of the GS specimen is larger than that of the PC specimen. This indicates that the energy consumption of each hysteresis loop of the GS specimen is larger than that of the PC specimen under the same rotation angle of the pier bottom condition.

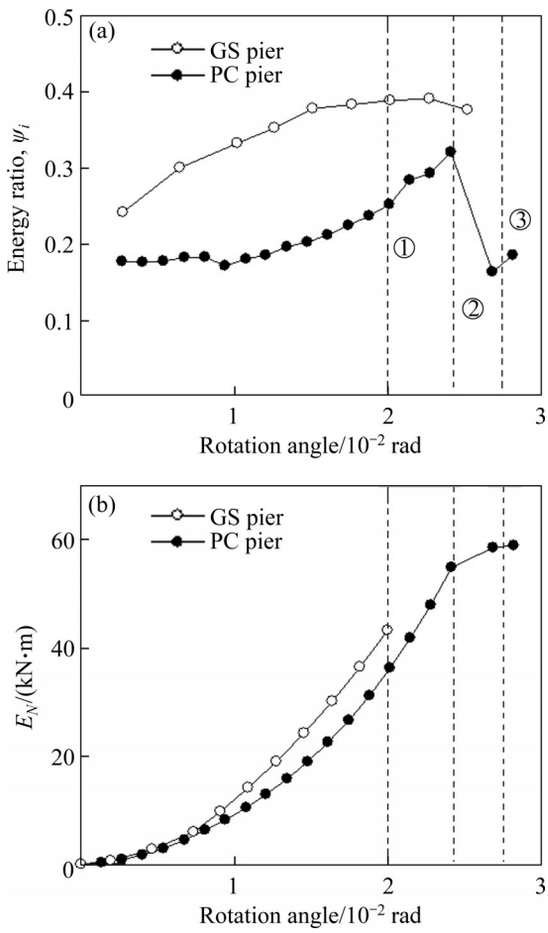

Figure 10 Energy dissipation capacity: (a) The relationship of energy ratio with rotation angle; (b) The relationship of hysteretic energy with rotation angle

The normalized cumulative hysteretic energy E_N is expressed as $E_N = \dfrac{1.0}{F_{\text{m}}\delta_y \sum_{i=1}^{N} E_i}$, where N is the total number of the loading cycles.

The variation of the E_N with rotation angle is shown in Figure 10. It can be noted that the E_N of the two pier specimens increases with the increase of the rotation angle at the bottom of the pier specimen. The E_N of the GS specimen is larger than the one of the PC specimen under the same rotation angle, which indicates that the GS specimen presents a good energy dissipation capacity. The PC

specimen cannot provide such a capacity as the longitudinal reinforcement does not run through the whole pier. Moreover, when the prestressed tendons break, the energy dissipation capacity of the pier will drop suddenly. As the concrete and longitudinal reinforcement bars enter the limit state one after another, the energy dissipation capacity of the PC specimen is completely provided by the prestressed tendons.

4.2.5 Residual displacement

Residual displacement index (RDI) is defined as the ratio of the residual displacement to δ_y. Figure 11 shows the RDI at different rotation angle levels for both specimens. The residual displacement of the PC specimen is very small, being only half of that of the GS specimen until the three prestressed tendons yield. The deployment of post-tensioned tendons can effectively reduce the residual displacement, as the prestressed force contributes to the increase of the self-centering capability.

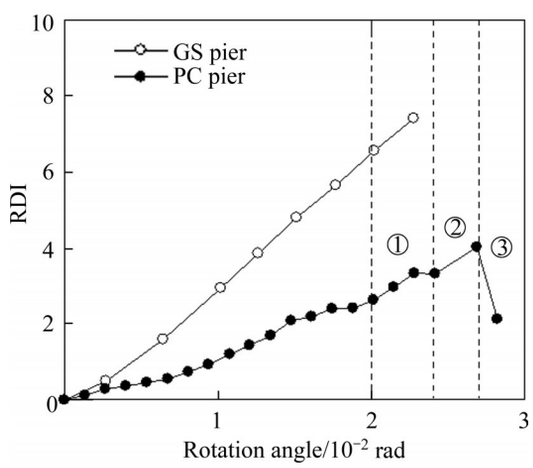

Figure 11 Comparison of residual displacement index

5 Numerical analysis

In this paper, the fiber finite element model is used to verify the hysteretic capacity of the GS and PC specimens, as shown in Figures 12 and 13. The lumped-mass model is adopted. The mass of the segmental column is lumped at the top of the column. The cap beam is simulated by the elastic beam element model. Concrete column segments are simulated by using the DispBeamColumn fiber element. Their cross section consists of cover concrete fibers, core concrete fibers, reinforced concrete fibers, longitudinal bar fibers and

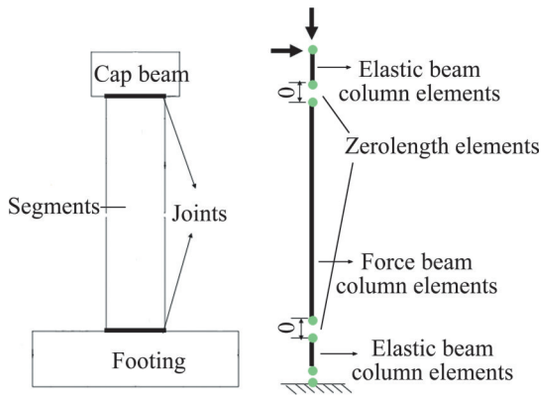

Figure 12 Fiber element model of the GS pier

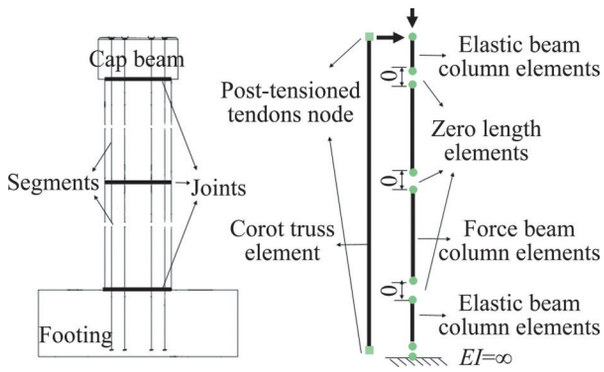

Figure 13 Fiber element model of the PC pier

prestressed tendons. The prestressed tendons are simulated by bar elements, and the pretension is introduced as an initial strain. The ZeroLength element is used to simulate the joints and calculate their hysteretic behavior. The constitutive relation of ZeroLength element is obtained by the experiment.

The hysteretic curves comparison between the experimental results and the numerical ones is shown in Figure 14. It is noted that:

1) For the GS pier, the residual displacement measured by the test is smaller than the numerical one. This is mainly due to the vertical load exerted by prestressed tendon in the test. In the process of applying horizontal displacement, the prestressing tendon produces a certain restoring force due to stretching.

2) For both the GS pier and the PC pier specimens, the numerical results and the experimental ones are not consistent in the negative direction of the hysteresis curve. This is mainly due to the fact that after the prototype pier has been reduced to a pier specimen, and the size and stiffness of the pier specimen are very small and sensitive to the change of load. The displacement

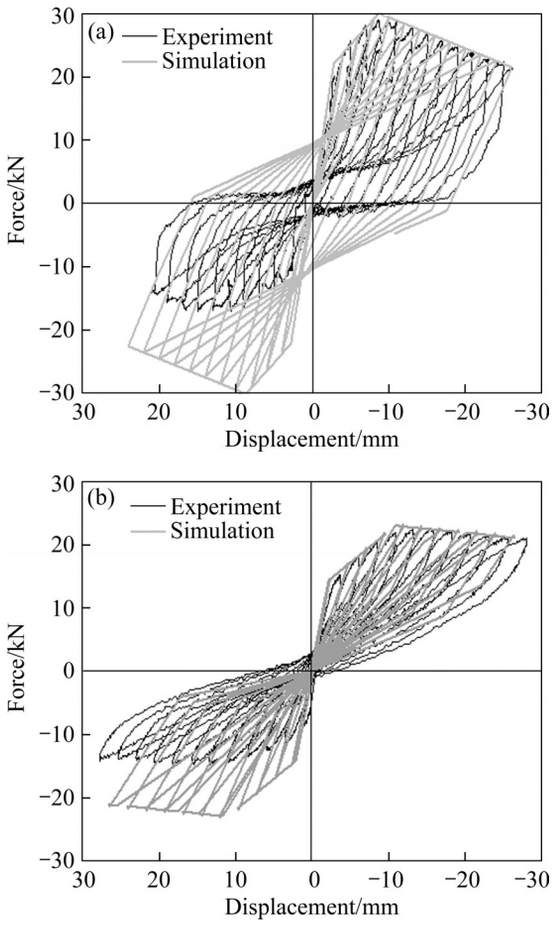

Figure 14 Comparison of numerical and experimental: (a) GS pier; (b) PC pier

load of each cycle is applied from the positive direction to the negative direction. In the unloading process, the stiffness of pier in negative direction is weakened.

Besides the above two problems, we can find that the numerical results and the test ones are in good agreement in the positive direction of the hysteretic curve.

6 Conclusions

In this paper, the seismic performance of precast assembled pier connected by grouting sleeve and prestressed tendons is compared through quasi-static test and numerical analyses under the same axial compression ratio. The following conclusions are drawn:

1) The failure modes of both GS and PC specimens show bending characteristics. However, the specific failure parts and forms are different. The GS specimen havs a failure mode similar to the one of the traditional cast-in-place pier, which is mainly manifested by the concrete crushing at the joint of the pier's base. The failure mode of the PC specimens is mainly concentrated in the rocking joints. The tensile damage of the precast components is reduced and the prefabricated components remain elastic.

2) The equivalent elastic stiffness of the two test piers is basically the same. Under the same load input, the GS specimen bottom segment is seriously damaged, the hysteresis loop is full, the residual displacement is large, the horizontal lateral stiffness is strong and the cumulative energy dissipation capacity is increased. Compared with the GS specimen, the PC specimen has a small damage, good self-reset ability, and poor energy consumption capacity, and can bear larger displacement.

3) Bond-slip behavior considered by implementing ZeroLength element at the joints can effectively improve the accuracy of the fiber element model. Before the bearing capacity drops to 85%, the differences between the experimental and numerical results are insignificant for both of GS and PC specimens.

Contributors

The overarching research goals were developed by WENLIUHAN Hei-sha. ZOU Shuang provided the test results. The initial draft of the manuscript was written by ZOU Shuang and WENLIUHAN Hei-sha. MAO Yong-ping, YU Bi-ping and ZHANG Chong-bin provided provision of test pier samples. All authors replied to reviewers' comments and revised the final version.

Conflict of interest

ZOU Shuang, WENLIUHAN Hei-sha, MAO Yong-ping, YU Bi-peng and ZHANG Chong-bin declare that they have no conflict of interest.

References

[1] ZHOU Yi-hui, OU Yu-chen, LEE G C. Bond-slip responses of stainless reinforcing bars in grouted ducts [J]. Engineering Structures, 2017, 141: 651–665. DOI: 10.1016/j. engstruct. 2017.03.049.

[2] LI Chao, HAO Hong, BI Kai-ming. Seismic performance of precast concrete-filled circular tube segmental column under biaxial lateral cyclic loadings [J]. Bulletin of Earthquake Engineering, 2019, 17(1): 271–296. DOI: 10.1007/s10518-

018-0443-4.

[3] TONG Teng, ZHUO Wei-ding, JIANG Xiao-fang, et al. Research on seismic resilience of prestressed precast segmental bridge piers reinforced with high-strength bars through experimental testing and numerical modelling [J]. Engineering Structures, 2019, 197: 109335. DOI: 10.1016/j.engstruct.2019.109335.

[4] BU Zhan-yu, OU Yu-chen, SONG Jian-wei, et al. Cyclic loading test of unbonded and bonded posttensioned precast segmental bridge columns with circular section [J]. Journal of Bridge Engineering, 2016, 21(2): 04015043. DOI: 10.1061/(asce)be.1943-5592.0000807.

[5] OU Yu-chen, CHIEWANICHAKORN M, AREF A J, et al. Seismic performance of segmental precast unbonded posttensioned concrete bridge columns [J]. Journal of Structural Engineering, 2007, 133(11): 1636−1647. DOI: 10.1061/(asce)0733-9445(2007)133: 11(1636).

[6] XIA Zhang-hua, GE Ji-ping, LIN You-qin, et al. Shake table study on precast segmental concrete double-column piers [J]. Earthquake Engineering and Engineering Vibration, 2020, 19(3): 705−723. DOI: 10.1007/s11803-020-0590-x.

[7] ZHANG Yu-ye, WU Gang, DIAS-DA-COSTA D. Cyclic loading tests and analyses of posttensioned concrete bridge columns combining cast-in-place and precast segments [J]. Bulletin of Earthquake Engineering, 2019, 17(11): 6141 − 6163. DOI: 10.1007/s10518-019-00714-0.

[8] LI Tian-tian, QU Hong-ya, WANG Zhi-qiang, et al. Seismic performance of precast concrete bridge columns with quasi-static cyclic shear test for high seismic zones [J]. Engineering Structures, 2018, 166: 441 − 453. DOI: 10.1016/j.engstruct.2018.03.086.

[9] ZHUO Wei-ding, LIU Zhao, ZHANG Jian-dong, et al. Comparison study on hysteretic energy dissipation and displacement components between cast-in-place and precast piers with high-strength bars [J]. Structural Concrete, 2018, 19(3): 747−757. DOI: 10.1002/suco.201700050.

[10] ICHINOSE T, KANAYAMA Y, INOUE Y, et al. Size effect on bond strength of deformed bars [J]. Construction and Building Materials, 2004, 18(7): 549 − 558. DOI: 10.1016/j.conbuildmat.2004.03.014.

[11] MURCIA-DELSO J, STAVRIDIS A, SHING P B. Bond strength and cyclic bond deterioration of large-diameter bars [J]. ACI Structural Journal, 2013, 110(4): 659−669.

[12] BU Zhan-yu, GUO Jian, ZHENG Rong-yue, et al. Cyclic performance and simplified pushover analyses of precast segmental concrete bridge columns with circular section [J]. Earthquake Engineering and Engineering Vibration, 2016, 15(2): 297−312. DOI: 10.1007/s11803-016-0323-3.

[13] KURAMA Y C, SRITHARAN S, FLEISCHMAN R B, et al. Seismic-resistant precast concrete structures: State of the art [J]. Journal of Structural Engineering, 2018, 144(4): 03118001. DOI: 10.1061/(asce)st.1943-541x.0001972.

[14] WANG Zhi-qiang, QU Hong-ya, LI Tian-tian, et al. Quasi-static cyclic tests of precast bridge columns with different connection details for high seismic zones [J]. Engineering Structures, 2018, 158: 13−17. DOI: https://doi.org/10.1016/j.engstruct.2017.12.035

[15] LU Zheng, WANG Zi-xin, LI Jian-bao, et al. Studies on seismic performance of precast concrete columns with grouted splice sleeve [J]. Applied Sciences, 2017, 7(6): 571. DOI: 10.3390/app7060571.

[16] LI Jian-bao, FAN Qiao-qiao, LU Zheng, et al. Experimental study on seismic performance of T-shaped partly precast reinforced concrete shear wall with grouting sleeves [J]. The Structural Design of Tall and Special Buildings, 2019, 28(13): e1632. DOI: 10.1002/tal.1632.

[17] HABER Z B, SAIIDI M S, SANDERS D H. Seismic performance of precast columns with mechanically spliced column-footing connections [J]. ACI Structural Journal, 2014, 111(3): 639−650. DOI: 10.14359/51686624.

[18] AMELI M J, PARKS J E, BROWN D N, et al. Seismic evaluation of grouted splice sleeve connections for reinforced precast concrete column-to-cap beam joints in accelerated bridge construction [J]. PCI Journal, 2015, 60(2): 80−103. DOI: 10.15554/pcij.03012015.80.103.

[19] HABER Z B, MACKIE K R, AL-JELAWY H M. Testing and analysis of precast columns with grouted sleeve connections and shifted plastic hinging [J]. Journal of Bridge Engineering, 2017, 22(10): 04017078. DOI: 10.1061/(asce)be.1943-5592.0001105.

[20] AMELI M J, PANTELIDES C P. Seismic analysis of precast concrete bridge columns connected with grouted splice sleeve connectors [J]. Journal of Structural Engineering, 2017, 143(2): 04016176. DOI: 10.1061/(asce)st.1943-541x.0001678.

[21] HABER Z B, SAIIDI M S, SANDERS D H. Behavior and simplified modeling of mechanical reinforcing bar splices [J]. ACI Structural Journal, 2015, 112(2): 179−188. DOI: 10.14359/51687455.

[22] QU Hong-ya, LI Tian-tian, WANG Zhi-qiang, et al. Investigation and verification on seismic behavior of precast concrete frame pier used in real bridge structures: Experimentatl and numerical study [J]. Engineering Structures, 2018, 154: 1 − 9. DOI: https://doi. org/10.1016/j.engstruct.2017.10.069.

[23] BILLINGTON S L, BARNES R W, BREEN J E. A precast segmental substructure system for standard bridges [J]. PCI Journal, 1999, 44(4): 56 − 73. DOI: 10.15554/pcij.07011999.56.73.

[24] LI Shuai, ZHAO Tai-yi, ALAM M S, et al. Probabilistic seismic vulnerability and loss assessment of a seismic resistance bridge system with post-tensioning precast segmental ultra-high performance concrete bridge columns [J]. Engineering Structures, 2020, 225(15): 111321. DOI: https://doi.org/10.1016/j.engstruct.2020.111321.

[25] HEWES J T, PRISTLEY M J N. Seismic design and performance of precast concrete segmental bridge columns [R]. San Diego: University of California at San Diego, 2002.

[26] GE Ji-ping, YAN Xing-fei, WANG Zhi-qiang. Seismic performance analysis of two-segment bridge columns with prestressing bars [J]. Journal of Railway Science and Engineering, 2017, 14(11): 2390−2398. DOI: 10.3969/j.issn.1672-7029.2017.11.017. (in Chinese)

[27] JIA Jun-feng, ZHAO Jian-yu, ZHANG Qiang, et al. Experiment on lateral bearing behavior of post-tensioned segmental CFST bridge pier columns [J]. China Journal of Highway and Transport, 2017, 30(3): 236 − 245. DOI: 10.19721/j.cnki.1001-7372.2017.03.026. (in Chinese)

[28] WANG Zhen, WANG Jing-quan, LIU Tong-xu. Axial compression ratio limit for self-centering precast segmental hollow piers [J]. Structural Concrete, 2017, 18(5): 668−679. DOI: 10.1002/suco.201600152.

[29] ZOU Shuang, WENLIUHAN H, ZHOU Fu-lin. Shaking table test of a high-speed railway bridge with a new isolation system [J]. Engineering Structures, 2019, 196: 109315. DOI: 10.1016/j.engstruct.2019.109315.

[30] YAO Qian-feng, CHEN Ping. Structural test of civil engineering [M]. Beijing: China Construction Industry Press, 2001. (in Chinese)

(Edited by HE Yun-bin)

中文导读

预制节段拼装混凝土双柱墩的抗震性能拟静力试验分析

摘要：本文以和田至若羌新建铁路项目中的灌浆套筒拼接与预应力节段预制拼接混凝土双柱墩为研究对象，通过实验室缩尺拟静力试验和数值分析，从破坏模式、承载力、延性、等效刚度和耗能能力等方面，对比研究了两种拼接形式双柱墩的抗震性能。研究结果表明，灌浆套筒拼接和预应力节段预制拼接双柱墩的破坏模式均为弯曲破坏。然而，灌浆套筒拼接桥墩的破坏模式与传统现浇桥墩相似，主要表现为墩底接缝处的混凝土压碎。预应力节段预制拼接桥墩的破坏主要表现为墩身与承台拼接处摇摆节点的形成。灌浆套筒拼接桥墩滞回曲线饱满，等效刚度大，耗能能力强。预应力节段预制拼接桥墩的滞回耗能较小，但是，它具有良好的自复位能力。用试验数据标定的基于位移的梁柱单元和零长单元建立的有限元模型可以有效地模拟单调加载下的装配式桥墩力学性能。

关键词：拟静力试验；抗震性能；灌浆套筒连接；预应力节段预制拼接；混凝土双柱墩；纤维单元模型